Rbf-Fd Solution with the Level-Set Embedded Boundary Method for the Diffusive Logistic Model with a Free Boundary

Chunyan Zhang and Yuanyang Qiao *

Posted Date: 19 January 2024

doi: 10.20944/preprints202401.1500.v1

Keywords: diffusive logistic model; moving boundary; embedded boundary method; RBF-FD; HJ-WENO; level set

Article

RBF-FD Solution with the Level-Set Embedded Boundary Method for the Diffusive Logistic Model with a Free Boundary

Chunyan Zhang and Yuanyang Qiao*

College of Mathematics and System Science, Xinjiang University, Urumqi 830017, P.R.China; 107552100531@stu.xju.edu.cn(C.Z.); qiaoyymath@126.com(Y.Q.)

* Correspondence: qiaoyymath@126.com

† These authors contributed equally to this work.

Abstract: In this paper, we propose an efficient numerical method to solve the diffusive logistic model with a free boundary which is often used to simulate the spreading of the new or invasive species. The boundary movement is tracked by the level-set method, where the Hamilton-Jacobi weighted essentially nonoscillatory (HJ-WENO) scheme is utilized to capture the boundary curve embedded by the Cartesian grids via the embedded boundary method. Then the radial basis function-finite difference (RBF-FD) method is adopted to the spatial discretization and the IMEX scheme is considered for time integration. A variety of numerical examples are carried out to demonstrate the evolution of diffusive logistic model in different initial boundaries.

Keywords: diffusive logistic model; moving boundary; embedded boundary method; RBF-FD; HJ-WENO; level set

1. Introduction

The diffusive logistic model with a free boundary, commonly used to describe the spreading of the new or invasive species in ecology, is acted as the moving boundary problems. The moving boundary problems originate from physical and engineering problems [7,28] and more recently from decision, control theory, and ecology [8], the details can be referred to Crank's research [28]. The key characteristic of moving boundary problems is that the boundary of the domain is unknown but is determined by the governing equation. More precisely, the behavior of a moving boundary is strongly related to that of an unknown solution.

The first diffusive logistic model related to ecological invasion began in 1937, without boundary constraints, and was independently proposed by Fisher [10] and Kolmogorov-Petrovsky-Piskunov (KPP) [17]. To the best of our knowledge, Du and Lin used the Stefan condition and solved the moving boundary problem of parabolic partial differential equations (PDEs) [8], which is the first exploration in the field of population diffusion. In particular, the spreading-vanishing dichotomy of the one-dimensional case was demonstrated. The regularity and asymptotic behavior of moving boundary $\partial\Omega(t)$ and the solution $u(\mathbf{x}, t)$ in high dimensions was studied in [9].

When numerically solving such a system, the main challenge arises from handling moving boundaries. To overcome this challenge and accurately measure both inner and outer regions, the embedded boundary method [14,25] is commonly employed. This method involves embedding the complex geometry into a Cartesian mesh, which allows for the discretization of the intricate geometric regions. By incorporating the boundary into the computational domain, the embedded boundary method effectively addresses the difficulties associated with moving boundaries.

Moreover, to overcome the limitations of traditional grid-based methods, researchers have explored alternative approaches that offer greater flexibility and efficiency. One such approach is the use of radial basis functions (RBF) for multidimensional discrete data interpolation. In non-convex regions, where boundaries exhibit complex shapes and changes, radial basis function interpolation enables to be highly adaptable for moving boundaries and irregular geometries, providing accurate

 doi:10.20944/preprints202401.1500.v1

interpolation results. Initially, RBF was used for global interpolation to solve PDEs, which was proposed by Kansa [15,16]. Global interpolation is easy to program and has spectral accuracy, but the resulting linear system is ill-conditioned. In order to solve this shortcoming, local interpolation [3–5,12] is proposed. Among them, the radial basis function finite difference (RBF-FD) is popular. It is accurate, robust, computationally efficient, and geometrically flexible. Notably, the RBF-FD method stands out for its ability to handle irregular and evolving domains. Unlike grid-based methods that require a structured mesh, the RBF-FD method operates on scattered nodes, allowing greater flexibility in representing complex geometries. In recent years, the RBF-FD method has been used to solve surface PDEs and has been applied to ecology, chemistry, geography, etc. [1,11,27].

In order to effectively deal with moving boundaries, the front-fixing method [20,21,26], the front-tracking method [18,20,21], and the level set method [6,20,21,23,24] are three popular numerical methods. The front-fixing method is relatively simple and easy to implement compared to other methods. However, its accuracy in simulating material interfaces with complex shape changes and internal structures may be limited. The front tracking method is proposed to address the one-dimensional problem and the level set method to handle the moving boundary for the two-dimensional problem by Liu et al. in [19,20]. Additionally, the front tracking algorithm is also employed to solve a two-dimensional model with radial symmetry in [18]. The level set method is generally robust in dealing with complex topological changes. When dealing with high-dimensional topological bifurcations, the level set method enables to be more effective in handling moving boundaries compared to the front-tracking method [21]. In practice, the level set function is commonly used as the indicator function of the boundary when tracking its motion, and the corresponding boundary equation is typically solved using the Hamilton-Jacobi weighted essentially nonoscillatory (HJ-WENO) scheme [13]. The purpose of this paper is to solve the diffusive logistic model with moving boundaries. The embedded boundary method is employed to establish a fixed computational domain that distinguishes the interior and exterior regions. The interior of the domain is discretized using the radial basis function finite difference method. Simultaneously, the boundary equation is solved by the HJ-WENO scheme, which determines the evolution of the moving boundary.

The rest of the paper is organized as follows. Section 2 presents the diffusive logistic model with a free boundary. In Section 3, the RBF-FD method is briefly reviewed, and the embedded boundary method for handling complex domains is presented. The numerical scheme for solving the diffusive logistic model with a stationary boundary is also given. The HJ-WENO scheme is introduced in Section 4, which is used to solve the level set equation. Additionally, the numerical algorithm for solving the diffusive logistic moving boundary problem is presented. Then in Section 5, the convergence test for the embedded boundary method is demonstrated. Various numerical examples are performed to track the evolution of the moving boundary in different initial boundaries. Finally, we come to the conclusion in Section 6.

2. Problem Formulation

The diffusive logistic model has been widely used in the simulation for the spreading of a new or invasive species with the free boundary representing the expanding front, it reads that

$$\frac{\partial u}{\partial t} - \gamma \Delta u = u(a - bu), \quad t > 0, \ \mathbf{x} \in \Omega(t), \tag{1}$$

subject to the boundary condition:

$$u(\mathbf{x}, t) = 0, \quad t > 0, \ \mathbf{x} \in \partial\Omega(t), \tag{2}$$

the Stefan condition:

$$\rho_t - \mu \nabla u \cdot \nabla \rho = 0, \quad t > 0, \ \mathbf{x} \in \Omega(t), \tag{3}$$

Preprints (www.preprints.org) | NOT PEER-REVIEWED | Posted: 19 January 2024 doi:10.20944/preprints202401.1500.v1

and the initial conditions:

$$\rho(\mathbf{x},0)=\rho_0(\mathbf{x}),\ u(\mathbf{x},0)=u_0(\mathbf{x}),\quad \mathbf{x}\in\Omega(0), \tag{4}$$

where $\gamma>0$ is the diffusive rate and $a>0$ and $b>0$ represent the intrinsic growth rate and the intraspecific competition, respectively. The initial function $u_0(\mathbf{x})$ satisfies the following regularity condition:

$$u_0(\mathbf{x})\in C^2(\Omega(0)),\ u_0(\mathbf{x})>0,\quad \mathbf{x}\in\Omega(0). \tag{5}$$

In the Stefan condition, ρ represents the indicator function of the boundary as follows:

$$\rho(\mathbf{x},t)=\begin{cases}+D, & \mathbf{x}\in\Omega(t)^c,\\ 0, & \mathbf{x}\in\partial\Omega(t),\\ -D, & \mathbf{x}\in\Omega(t),\end{cases} \tag{6}$$

where D represents the Euclidean distance between the point $\mathbf{x}$ and the boundary $\partial\Omega(t)$. The idea of introducing the level set function is that the boundary is equal to the zero level set at any given time, i.e.,

$$\partial\Omega(t)=\{\mathbf{x}\mid\rho(\mathbf{x},t)=0\}, \tag{7}$$

where $\partial\Omega(t)$ denotes the boundary of Ω at time t. $\mu>0$ denotes the proportionality constant between the species gradient at the front and the speed of the moving boundary.

3. Embedded Boundary Method with the RBF-FD Discretization

In this part, we give a brief review on the RBF-FD discretization for the given differential operator, then embedded boundary method is presented to treat the complex domain and an IMEX scheme is considered for the time integration of diffusive logistic model with the stationary boundary.

3.1. RBF-FD Discretization

Given a differential operator $\mathcal{L}$. Select the stencil $\{\mathbf{x}_i\}_{i=1}^n$ centered on point $\mathbf{x}_1$ where n is the stencil size, then $\mathcal{L}u$ can be approximately expressed as a linear combination of the values of the functions at each stencil point, i.e.,

$$\mathcal{L}u(\mathbf{x})|_{\mathbf{x}=\mathbf{x}_1}\approx\sum_{i=1}^{n}w_iu(\mathbf{x}_i), \tag{8}$$

where $w_1,w_2,\ldots,w_n$ are a set of weight coefficients.

Through the above stencil points $\mathbf{x}_1,\mathbf{x}_2,\ldots,\mathbf{x}_n$ and the function values $u(\mathbf{x}_1),u(\mathbf{x}_2),\ldots,u(\mathbf{x}_n)$ at the corresponding nodes, we use the following radial basis function coupled polynomial interpolation:

$$u_h(\mathbf{x})=\sum_{j=1}^{n}c_j\phi(\|\mathbf{x}-\mathbf{x}_j\|)+\sum_{i=1}^{m}\lambda_iP_i(\mathbf{x}), \tag{9}$$

subject to:

$$\sum_{j=1}^{n}c_jP_i(\mathbf{x}_j)=0,\qquad i=1,2,\ldots,m, \tag{10}$$

where $c_1,c_2,\ldots,c_n$ and $\lambda_1,\lambda_2,\ldots,\lambda_m$ are undetermined coefficients. $\phi(\|\mathbf{x}-\mathbf{x}_j\|)$ is the radial basis function and $\|\cdot\|$ represents the Euclid distance. $\{P_i\}_{i=1}^m$ is the polynomial basis where m is the number

Preprints (www.preprints.org) | NOT PEER-REVIEWED | Posted: 19 January 2024 doi:10.20944/preprints202401.1500.v1

of polynomial bases. The calculation formula of m is $m = \binom{p+d}{p}$, p is the highest degree of polynomial, and d is the space dimension. On the one hand, the addition of polynomial terms ensures that the radial function and polynomial space together form a complete space, preventing the matrix from being singular. On the other hand, this approach guarantees that the interpolation accuracy reaches at least polynomial accuracy.

Let $\phi_j(\mathbf{x}) = \phi(\|\mathbf{x} - \mathbf{x}_j\|)$ and $p = 2$. The polynomial basis functions are given by $\{1, x, y, x^2, xy, y^2\}$. According to the interpolation condition $u_h(\mathbf{x}_i)|_{i=1}^n = u(\mathbf{x}_i)|_{i=1}^n$, we can obtain a linear system:

$$\begin{bmatrix} \phi_1(\mathbf{x}_1) & \phi_2(\mathbf{x}_1) & \cdots & \phi_n(\mathbf{x}_1) & 1 & x_1 & \cdots & y_1^2 \\ \phi_1(\mathbf{x}_2) & \phi_2(\mathbf{x}_2) & \cdots & \phi_n(\mathbf{x}_2) & 1 & x_2 & \cdots & y_2^2 \\ \vdots & \vdots & \ddots & \vdots & \vdots & \vdots & \ddots & \vdots \\ \phi_1(\mathbf{x}_n) & \phi_2(\mathbf{x}_n) & \cdots & \phi_n(\mathbf{x}_n) & 1 & x_n & \cdots & y_n^2 \\ 1 & 1 & \dots & 1 & 0 & 0 & \dots & 0 \\ x_1 & x_2 & \dots & x_n & 0 & 0 & \dots & 0 \\ \vdots & \vdots & \ddots & \vdots & \vdots & \vdots & \ddots & \vdots \\ y_1^2 & y_2^2 & \dots & y_n^2 & 0 & 0 & \dots & 0 \end{bmatrix} \begin{bmatrix} c_1 \\ c_2 \\ \vdots \\ c_n \\ \lambda_1 \\ \lambda_2 \\ \vdots \\ \lambda_m \end{bmatrix} = \begin{bmatrix} u(\mathbf{x}_1) \\ u(\mathbf{x}_2) \\ \vdots \\ u(\mathbf{x}_n) \\ 0 \\ 0 \\ \vdots \\ 0 \end{bmatrix}, \tag{11}$$

or equivalently, it can be written as the matrix form

$$\begin{bmatrix} A & P \\ P^T & 0 \end{bmatrix} \begin{bmatrix} \mathbf{c} \\ \boldsymbol{\lambda} \end{bmatrix} = \begin{bmatrix} \mathbf{u} \\ 0 \end{bmatrix}, \tag{12}$$

where $\mathbf{c} = (c_1, c_2, \dots, c_n)^T$, $\boldsymbol{\lambda} = (\lambda_1, \lambda_2, \dots, \lambda_m)^T$, $\mathbf{u} = (u(\mathbf{x}_1), u(\mathbf{x}_2), ..., u(\mathbf{x}_n))^T$, A is the coefficient matrix of the radial basis function, and P is the coefficient matrix of the polynomial basis.

$$A = \begin{bmatrix} \phi_1(\mathbf{x}_1) & \phi_2(\mathbf{x}_1) & \cdots & \phi_n(\mathbf{x}_1) \\ \phi_1(\mathbf{x}_2) & \phi_2(\mathbf{x}_2) & \cdots & \phi_n(\mathbf{x}_2) \\ \vdots & \vdots & \ddots & \vdots \\ \phi_1(\mathbf{x}_n) & \phi_2(\mathbf{x}_n) & \cdots & \phi_n(\mathbf{x}_n) \end{bmatrix}, P = \begin{bmatrix} 1 & x_1 & \cdots & y_1^2 \\ 1 & x_2 & \cdots & y_2^2 \\ \vdots & \vdots & \ddots & \vdots \\ 1 & x_n & \cdots & y_n^2 \end{bmatrix}.$$

It follows from the non-singularity of the interpolation matrix [27] that

$$\begin{bmatrix} \mathbf{c} \\ \boldsymbol{\lambda} \end{bmatrix} = \begin{bmatrix} A & P \\ P^T & 0 \end{bmatrix}^{-1} \begin{bmatrix} \mathbf{u} \\ 0 \end{bmatrix}. \tag{13}$$

Now we apply the differential operator $\mathcal{L}u(\mathbf{x})|_{\mathbf{x}=\mathbf{x}_1}$ to the interpolation formula to obtain the differential relation:

$$\begin{aligned} \mathcal{L}u(\mathbf{x})|_{\mathbf{x}=\mathbf{x}_1} &\approx \mathcal{L}u_h(\mathbf{x})|_{\mathbf{x}=\mathbf{x}_1} \\ &= \sum_{j=1}^{n} c_j \mathcal{L}\phi_j(\mathbf{x})|_{\mathbf{x}=\mathbf{x}_1} + \sum_{i=1}^{m} \lambda_i \mathcal{L}P_i(\mathbf{x})|_{\mathbf{x}=\mathbf{x}_1} \\ &= \begin{bmatrix} \mathcal{L}\phi(\mathbf{x})^T|_{\mathbf{x}=\mathbf{x}_1} & \mathcal{L}P(\mathbf{x})^T|_{\mathbf{x}=\mathbf{x}_1} \end{bmatrix} \begin{bmatrix} \mathbf{c} \\ \boldsymbol{\lambda} \end{bmatrix} \\ &= \begin{bmatrix} \mathcal{L}\phi(\mathbf{x})^T|_{\mathbf{x}=\mathbf{x}_1} & \mathcal{L}P(\mathbf{x})^T|_{\mathbf{x}=\mathbf{x}_1} \end{bmatrix} \begin{bmatrix} A & P \\ P^T & 0 \end{bmatrix}^{-1} \begin{bmatrix} \mathbf{u} \\ 0 \end{bmatrix} \\ &= \begin{bmatrix} \mathbf{w}^T & \boldsymbol{\beta}^T \end{bmatrix} \begin{bmatrix} \mathbf{u} \\ 0 \end{bmatrix} = \mathbf{w}^T \mathbf{u}, \end{aligned} \tag{14}$$

Preprints (www.preprints.org) | NOT PEER-REVIEWED | Posted: 19 January 2024 doi:10.20944/preprints202401.1500.v1

where $\mathcal{L}\phi(\mathbf{x}) = \{\mathcal{L}\phi_j(\mathbf{x})\}_{j=1}^n$ and $\mathcal{L}P(\mathbf{x}) = \{\mathcal{L}P_i(\mathbf{x})\}_{i=1}^m$. The above equation can also deduce a weight formula:

$$\begin{bmatrix} \mathcal{L}\phi^T & \mathcal{L}P^T \end{bmatrix} \begin{bmatrix} A & P \\ P^T & 0 \end{bmatrix}^{-1} = \begin{bmatrix} \mathbf{w}^T & \boldsymbol{\beta}^T \end{bmatrix},$$

which in turn implies that

$$\begin{bmatrix} A & P \\ P^T & 0 \end{bmatrix} \begin{bmatrix} \mathbf{w} \\ \boldsymbol{\beta} \end{bmatrix} = \begin{bmatrix} \mathcal{L}\phi \\ \mathcal{L}P \end{bmatrix}.$$

It is worth noting that the above computational process of weight coefficients only need to retain $\mathbf{w}$. When the differential weights are obtained, we can discretize the differential operator by substituting it back to (8).

3.2. Embedded Boundary Method

The idea of the embedded boundary condition is to embed the complex geometry into the Cartesian mesh covering the entire computational domain. To this end, we recall the diffusive logistic model with the stationary boundary

$$\frac{\partial u}{\partial t} - \gamma \Delta u = u(a - bu), \quad t > 0, \ \mathbf{x} \in \Omega,$$

subject to the boundary condition:

$$u(\mathbf{x}, t) = 0, \quad t > 0, \ \mathbf{x} \in \partial\Omega,$$

and the appropriate initial condition:

$$u(\mathbf{x}, 0) = u_0(\mathbf{x}), \quad \mathbf{x} \in \Omega.$$

Assume Ω is contained inside a rectangular domain $\widetilde{\Omega} = [0, L_1] \times [0, L_2]$, and for simplify, let $L_1 = L_2 = L$. Denote N as an integer, let us discretize the spatial domain Ω by a uniform mesh with the spatial step size $h = L/N$ as follows

$$\widetilde{\Omega}_h = \{(x_i, y_j) | x_i = ih, y_j = jh, 0 \le i, j \le N\}. \tag{15}$$

Denote $T > 0$ as the terminal time, let $t_n = n\tau$, $0 \le n \le T/\tau$, where τ is the time step size. Let $u_{i,j}^n = u_{i,j}(t_n)$ be the numerical approximation of u in the mesh point (x_i, y_j) at time $t = t_n$.

Applying the spatial discresization via the RBF-FD method as in previous subsection for the Laplacian operator Δ, denoted by Δ_h, the corresponding space-discrete equation becomes an ordinary differential equation

$$\frac{\partial u}{\partial t} - \gamma \Delta_h u = u(a - bu),$$

and then an IMEX scheme is considered for time integration

$$\frac{u^{n+1} - u^n}{\tau} - \gamma \Delta_h u^{n+1} = u^n(a - bu^n). \tag{16}$$

4. Level Set Method with the HJ-WENO Scheme

A level set function is utilized to capture the boundary movement. The governing equation determining the evolution of boundary is given by

$$\begin{cases} \rho_t - \mu \nabla u \cdot \nabla \rho = 0, & t > 0, \mathbf{x} \in \widetilde{\Omega}, \\ \rho(\mathbf{x}, 0) = \rho_0(\mathbf{x}), & \mathbf{x} \in \widetilde{\Omega}, \end{cases} \tag{17}$$

Preprints (www.preprints.org) | NOT PEER-REVIEWED | Posted: 19 January 2024 doi:10.20944/preprints202401.1500.v1

where $\widetilde{\Omega}$ is the computational domain derived by the embedded boundary method. Level set Equation (17) can be regarded as the special case of the Hamilton-Jacobi (HJ) equation, where $-\mu\nabla u\cdot\nabla\rho$ is the Hamitonian. Thus the HJ-WENO scheme can be used to discretize the level set equation.

Denote $H(\rho_x,\rho_y)=-\mu\nabla u\cdot\nabla\rho=-\mu u_x\rho_x-\mu u_y\rho_y$, the level set equation can be discretized in the following form [13]:

$$\frac{d\rho_{i,j}}{dt}=-\hat{H}(\rho^+_{x,i,j},\rho^-_{x,i,j},\rho^+_{y,i,j},\rho^-_{y,i,j}), \tag{18}$$

where $\rho^-_{x,i,j}$ and $\rho^+_{x,i,j}$ are the approximate values of $\rho_x(x_i,y_j)$ obtained on the left and right stencils illustrated in Figure 1, respectively. $\rho^+_{y,i,j}$ and $\rho^-_{y,i,j}$ are similar. $\hat{H}$ is a Lipschitz continuous monotone flux, which is consistent with the Hamiltonian H, i.e., $\hat{H}(\rho^+_x,\rho^-_x,\rho^+_y,\rho^-_y)=H(\rho_x,\rho_y)$. In this paper, we use the Lax-Friedrichs (LF) flux:

$$\hat{H}(\rho^+_x,\rho^-_x,\rho^+_y,\rho^-_y)=H(\frac{\rho^+_x+\rho^-_x}{2},\frac{\rho^+_y+\rho^-_y}{2})-\alpha(\rho^+_x,\rho^-_x)\frac{\rho^+_x-\rho^-_x}{2}-\beta(\rho^+_y,\rho^-_y)\frac{\rho^+_y-\rho^-_y}{2}$$

with

$$\alpha(\rho^+_x,\rho^-_x)=\max_{\rho_x\in I(\rho^-_x,\rho^+_x)}|H'(\rho_x)|=\mu\max_{\mathbf{x}\in\widetilde{\Omega}}|u_x|,$$
$$\beta(\rho^+_y,\rho^-_y)=\max_{\rho_y\in I(\rho^-_y,\rho^+_y)}|H'(\rho_y)|=\mu\max_{\mathbf{x}\in\widetilde{\Omega}}|u_y|,$$

where $I(a,b)=[\min(a,b),\max(a,b)]$.

In the same way, we also get the approximate value $u^+_{x,i,j}$, $u^-_{x,i,j}$, $u^+_{y,i,j}$, $u^-_{y,i,j}$ of $u_x(x_i,y_j)$ and $u_y(x_i,y_j)$ by the fifth-order HJ-WENO reconstruction. Then we obtain

$$u_{x,i,j}=\omega u^+_{x,i,j}+(1-\omega)u^-_{x,i,j}, \tag{19}$$

where $\omega\in[0,1]$ is the weight coefficient. Similarly, $u_{y,i,j}$ can be obtained. After the overall reconstruction, we adopt the TVD scheme to the semi-discrete system

$$\begin{aligned}\frac{\rho^{n+1}_{i,j}-\rho^n_{i,j}}{\tau}=&\mu u^n_{x,i,j}\frac{\rho^{n,+}_{x,i,j}+\rho^{n,-}_{x,i,j}}{2}+\mu u^n_{y,i,j}\frac{\rho^{n,+}_{y,i,j}+\rho^{n,-}_{y,i,j}}{2}\\&+\alpha(\rho^{n,+}_{x,i,j},\rho^{n,-}_{x,i,j})\frac{\rho^{n,+}_{x,i,j}-\rho^{n,-}_{x,i,j}}{2}+\beta(\rho^{n,+}_{y,i,j},\rho^{n,-}_{y,i,j})\frac{\rho^{n,+}_{y,i,j}-\rho^{n,-}_{y,i,j}}{2}\\:=&L(\rho^n_{i,j},u^n_{i,j}).\end{aligned} \tag{20}$$

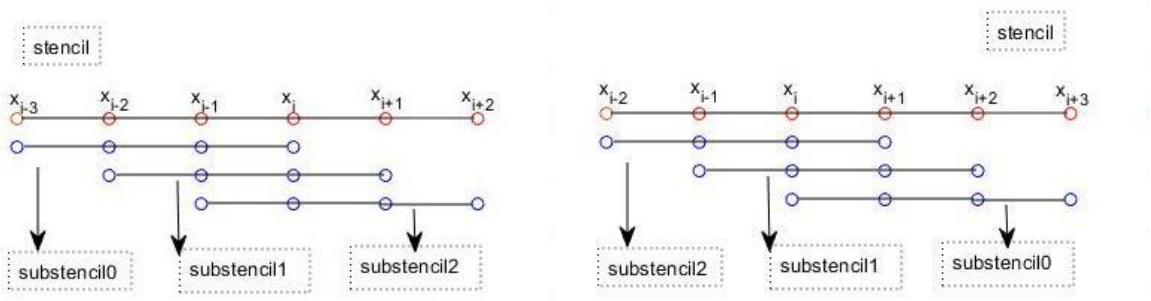

Figure 1. The left-biased stencil and the right-biased stencil.

Preprints (www.preprints.org) | NOT PEER-REVIEWED | Posted: 19 January 2024 doi:10.20944/preprints202401.1500.v1

For the moving boundary problem described in (1), it is challenging to solve the diffusive logistic model accurately and effectively due to the evolving computational boundary over time. We will couple with the embedded boundary method and level set method to develop an efficient numerical scheme. The details are followed by

Algorithm.

- **Step 1**: Set a sufficient large rectangular domain $\widetilde{\Omega} \subset R^2$, so that the whole irregular area $\Omega(t) \subset \widetilde{\Omega}$ for $t \in [0, T]$. Initialize the level set function ρ^0 and u^0. Set $n = 0$.
- **Step 2**: Solve (16) over $\widetilde{\Omega}$ to obtain u^{n+1}.
- **Step 3**: Solve (20) over $\widetilde{\Omega}$ to obtain ρ^{n+1}.
- **Step 4**: Set $n := n + 1$. Steps 1-2 are repeated over time until the final simulation time is reached.

5. Numerical Experiments

In this part, we perform the simulation on the evolution process of the moving boundary in various regions. The polyharmonic splines (PHS) radial basis function with $\phi(r) = r^5$ augmented with the quadratic polynomial is adopted to the RBF-FD spatial discretization, which does not need to determine the shape parameters and thus simplifies the calculation compared with the other parameters-determined radial basis functions, see [2]. And the closest point method is utilized to select the stencil point where the number of stencil points is 13 around the central node. The embedded computational domain is always chosen as $[-1, 1]^2$ in two-dimensional space.

5.1. Convergence Test for Embedded Boundary Method

In this example, we consider the Poisson equation $\nabla \cdot (c(x, y)\nabla u) = f(x, y)$ in an irregular domain Ω, which is determined by the parameterized boundary interface:

$$\begin{cases} \rho = r - (0.5 + 0.2\sin(5\theta)), \\ \theta = \arctan(y/x), \\ r = \sqrt{x^2 + y^2}, \end{cases}$$

with the exact solution $u = e^x + e^y$. The diffusion coefficient $c(x, y) = 2 + \sin(xy)$ and the forcing term $f(x, y)$ is computed by the exact solution.

Convergence results of the solution for the two-dimensional variable coefficient Poisson equation are shown in Table 1, which reports the spatial error in L^2 norm and L^∞ norm and the corresponding convergence rate. The numerical solution and the numerical error with $N = 1280$ are presented in Figure 2. It can be observed that the spatial convergence rate of the embedded boundary method is of second order, which is consistent with the quadratic polynomial.

Table 1. Spatial error in L^2 norm and L^∞ norm and corresponding convergence rate.

N	L^2 Error	Rate	L^∞ Error	Rate
40	6.0670e–06	-	1.3948e–05	-
80	1.4202e–06	2.09	3.3572e–06	2.05
160	3.4323e–07	2.05	8.2027e–07	2.03
320	8.3416e–08	2.04	2.0084e–07	2.03
640	2.0532e–08	2.02	4.9634e–08	2.02
1280	5.1003e–09	2.01	1.2351e–08	2.01

Preprints (www.preprints.org) | NOT PEER-REVIEWED | Posted: 19 January 2024 doi:10.20944/preprints202401.1500.v1

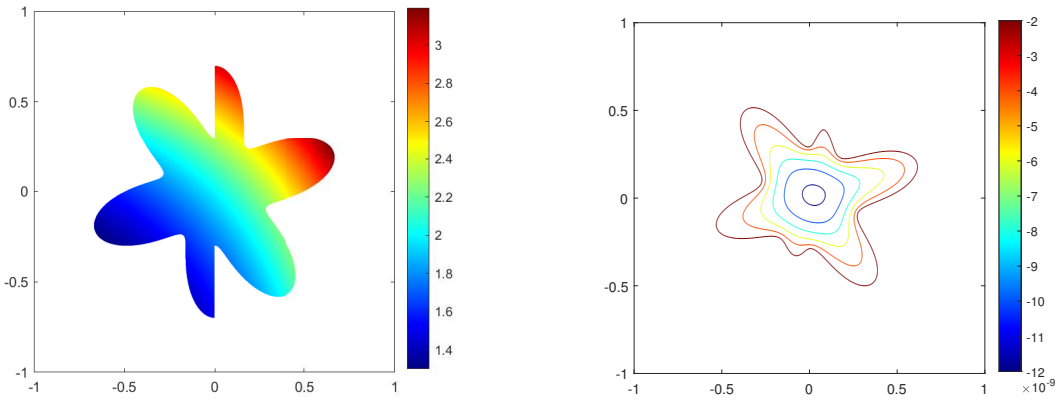

Figure 2. Profiles of Numerical Solution (Left) and Error (Right) on the Irregular Domain with $N = 1280$.

5.2. Numerical Tests for Diffusive Logistic Model with a Free Boundary

In this part, we next consider the diffusive logistic model (1) with the different parameter settings in the specific initial value and initial level set function. The time-space step size is always set as $\tau = 1e-4$ and $h = 1/40$. The terminal time is $T = 0.1$.

Example 1. *The initial boundary is set as a circle where the center of the circle is at the origin point* $(0,0)$*, and the radius is* 0.5*, with the initial level set function given by*

$$\rho(x,y,0) = -(0.5 - \sqrt{x^2+y^2}). \tag{21}$$

The initial value is $u(x,y,0) = 5\cos(\sqrt{x^2+y^2}\pi)$*. The parameter settings are set as* $(\gamma,\mu,a,b) = (1,1,1,1)$.

Figure 3 shows the evolutions of the numerical solution and the moving boundary at t=0.0002, 0.0242, 0.0661 and 0.1, respectively. It can be seen that the circle propagates in the form of a circle and the circular area becomes larger and larger as time evolution which is in agreement with the results of [9].

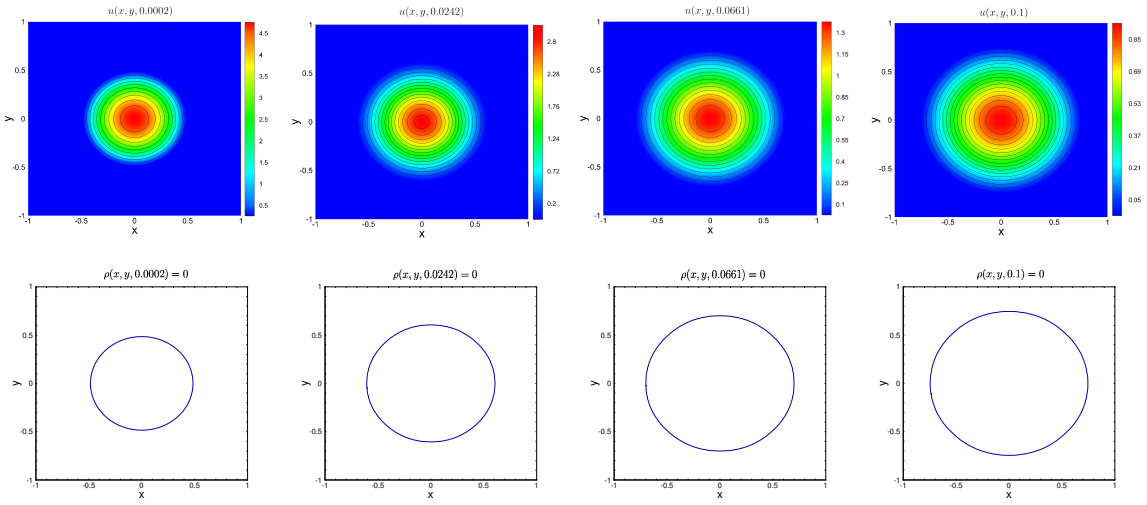

Figure 3. Evolutions of the numerical solution $u(x,y,t)$ and the moving boundary when the initial boundary is circular.

Preprints (www.preprints.org) | NOT PEER-REVIEWED | Posted: 19 January 2024 doi:10.20944/preprints202401.1500.v1

Example 2. *The initial boundary is set as a square where the center of the square is at the origin point* $(0,0)$*, and the side length is 0.6, with the initial level set function expressed as*

$$\rho(x,y,0) = -\min(0.3-|x|, 0.3-|y|). \tag{22}$$

The initial value is $u(x,y,0) = 100(0.3^2-x^2)(0.3^2-y^2)$*. The parameter settings are set as* $(\gamma,\mu,a,b) = (1,10,1,1)$*.*

Figure 4 shows the evolutions of the numerical solution and the moving boundary at t=0.0015, 0.0357, 0.0812 and 0.1, respectively. It can be observed that the initial square boundary eventually evolves into a circle and propagates in the form of a circle, which is consistent with that in [9].

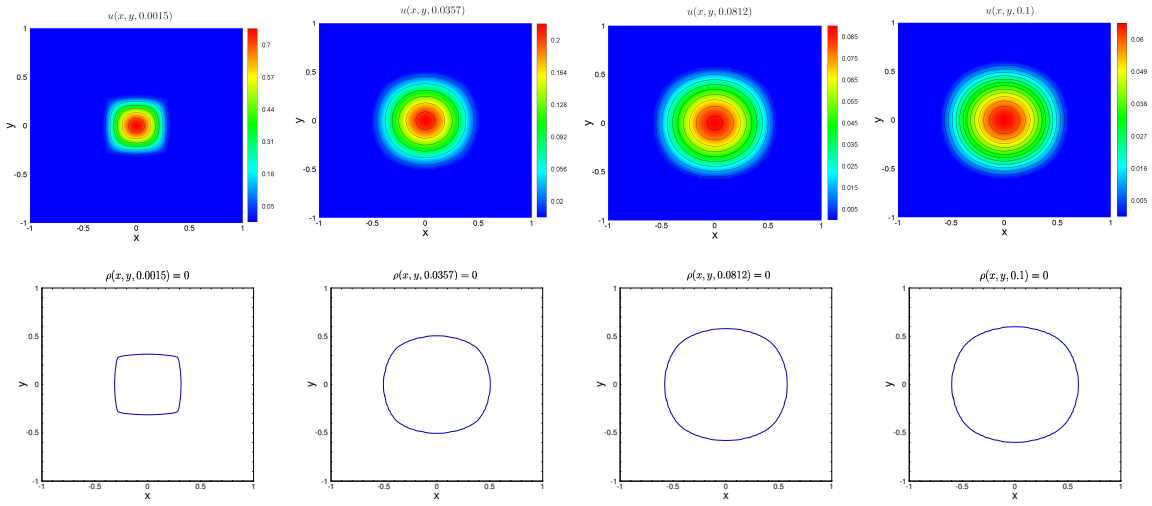

Figure 4. Evolutions of the numerical solution $u(x,y,t)$ and the moving boundary when the initial boundary is a square.

Example 3. *The initial boundary is set as an equilateral triangle centered at the origin point* $(0,0)$ *with a side length of 1, with the initial level set function defined by*

$$\rho(x,y,0) = -\min(\frac{\sqrt{3}}{2} - \frac{1}{\sqrt{3}} + y, \sqrt{3}x - y + \frac{1}{\sqrt{3}}, -\sqrt{3}x - y + \frac{1}{\sqrt{3}}). \tag{23}$$

The initial value is $u(x,y,0) = 10(\frac{\sqrt{3}}{2} - \frac{1}{\sqrt{3}} + y)(\sqrt{3}x - y + \frac{1}{\sqrt{3}})(-\sqrt{3}x - y + \frac{1}{\sqrt{3}})$*. The parameter settings are* $(\gamma,\mu,a,b) = (1,10,1,1)$*.*

Figure 5 shows the evolutions of the numerical solution and the moving boundary at t=0.0001, 0.0094, 0.0301 and 0.1, respectively, from which it can be observed that the moving boundary asymptotically evolves into a circle, which is consistent with the asymptotic behavior described in [9].

Preprints (www.preprints.org) | NOT PEER-REVIEWED | Posted: 19 January 2024 doi:10.20944/preprints202401.1500.v1

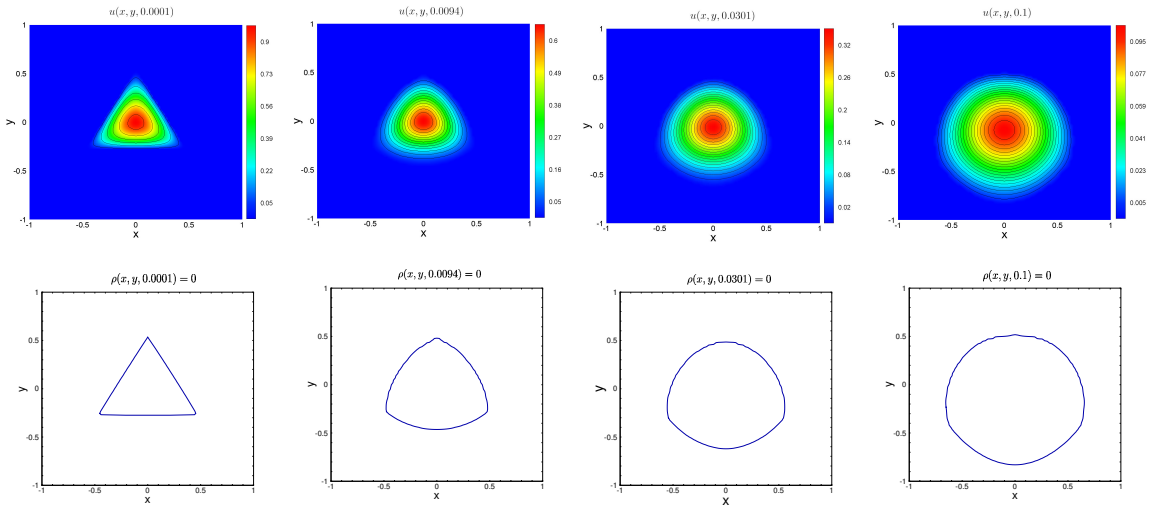

Figure 5. Evolutions of the numerical solution $u(x, y, t)$ and the moving boundary when the initial boundary is a triangle.

Example 4. *The initial boundary is set as a rectangle with the two adjacent sides measuring 0.6 and 0.8 respectively, with the initial level set function*

$$\rho(x, y, 0) = -\min(0.3 - |x|, 0.4 - |y|). \tag{24}$$

The initial value is $u(x, y, 0) = 100(0.3^2 - x^2)(0.4^2 - y^2)$. *The parameter settings are* $(\gamma, \mu, a, b) = (1, 10, 1, 1)$.

Figure 6 depicts the evolutions of the numerical solution and the moving boundary at t=0.0002, 0.0311, 0.0702 and 0.1, respectively, from which we can see that the boundary evolves into a circle and propagates gradually over time, which is in accordance with the prediction made in [9].

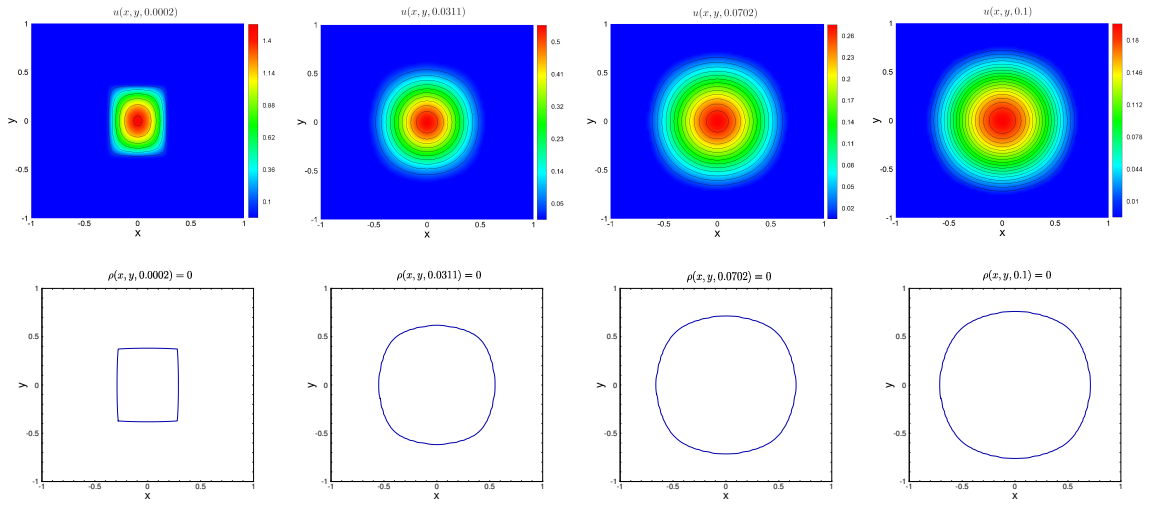

Figure 6. Evolutions of the numerical solution $u(x, y, t)$ and the moving boundary when the initial boundary is a rectangle.

6. Conclusions

In this paper, we have incorporated the embedded boundary method with the RBF-FD discretization and the level set method with the HJ-WENO scheme to systematically investigate the diffusive logistic model with a free boundary. Embedded boundary method embeds the moving boundary within a rectangular domain to facilitate the construction of the discrete scheme, in

which the spatial discretization is realized by the RBF-FD method. Additionally, the HJ-WENO scheme is employed to discretize the level set convection equation and thus the moving boundary is obtained. Various numerical experiments are conducted to demonstrate the capability and efficiency of the proposed scheme in treating the irregular geometry. Moreover, we can observe that moving boundaries with initial regions shaped as circles, squares, triangles, and rectangles undergo changes and asymptotically evolve into circular shapes over time. How to extend to more complex diffusive models with a free boundary will be our future research. Specifically, the more-component diffusive logistic model with a free boundary will be studied later.

Author Contributions: Conceptualization, C.Z. and Y.Q.; methodology, C.Z. and Y.Q.; software, Y.Q.; formal analysis, C.Z. and Y.Q.; investigation, C.Z.; writing—original draft preparation, C.Z.; writing—review and editing, C.Z. and Y.Q.; funding acquisition, Y.Q. All authors have read and agreed to the published version of the manuscript.

Funding: This research was funded by Natural Science Foundation of Xinjiang grant 2021D01C114, Lanzhou University Double-Class Project grant 561120207 and National Natural Science Foundation of China grant 12301510.

Institutional Review Board Statement: Not applicable.

Informed Consent Statement: Not applicable.

Data Availability Statement: Data are contained within the article.

Acknowledgments: The authors would like to express their sincere appreciation for Professor Jingwei Li's guidance from Lanzhou University and extend their thanks to the editors and reviewers for their invaluable suggestions.

Conflicts of Interest: The authors declare no conflicts of interest.

Abbreviations

The following abbreviations are used in this manuscript:

PHS	polyharmonic splines
IMEX	implicit-explicit
RBF-FD	radial basis function-finite difference
HJ-WENO	Hamilton-Jacobi weighted essentially nonoscillatory

References

1. Álvarez D, González-Rodríguez P, Kindelan M. A local radial basis function method for the Laplace-Beltrami operator. *J. Sci. Comput.* **2021**, *86*, 28.
2. Barnett, G.A. A robust RBF-FD formulation based on polyharmonic splines and polynomials. PhD Thesis, Citeseer, 2015.
3. Bayona V, Moscoso M, Carretero M, et al. RBF-FD formulas and convergence properties. *J. Comput. Phys.* **2010**, *229*, 8281–8295.
4. Bayona V, Moscoso M, Kindelan M. Optimal constant shape parameter for multiquadric based RBF-FD method. *J. Comput. Phys.* **2011**, *230*, 7384–7399.
5. Cecil T, Qian J, Osher S. Numerical methods for high dimensional Hamilton-Jacobi equations using radial basis functions. *J. Comput. Phys.* **2004**, *196*, 327–347.
6. Chen S, Merriman B, Osher S, et al. A simple level set method for solving Stefan problems. *J. Comput. Phys.* **1997**, *135*, 8–29.
7. Duffy D J. *Finite Difference methods in financial engineering: a Partial Differential Equation approach.*, John Wiley & Sons, 2013.
8. Du Y, Lin Z. Spreading-vanishing dichotomy in the diffusive logistic model with a free boundary. *SIAM J. Math. Anal.* **2010**, *42*,377–405.
9. Du Y, Matano H, Wang K. Regularity and asymptotic behavior of nonlinear Stefan problems. *Arch Ration Mech An.* **2014**, *212*,957–1010.
10. Fisher R A. The wave of advance of advantageous genes. *Annals of eugenics.* **1937**, *7*,355–369.

11. Flyer N, Fornberg B, Bayona V, et al. On the role of polynomials in RBF-FD approximations: I. Interpolation and accuracy. *J. Comput. Phys.* **2016**, *321*,21–38.
12. Fornberg B, Flyer N. Solving PDEs with radial basis functions. *Acta Numerica* **2015**, *24*,215–258.
13. Jiang G S, Peng D. Weighted ENO schemes for Hamilton-Jacobi equations. *SIAM J. Sci. Comput.* **2000**, *21*,2126–2143.
14. Johansen H, Colella P. A Cartesian grid embedded boundary method for Poisson's equation on irregular domains. *J. Comput. Phys.* **1998**, *147*,60–85.
15. Kansa E J. Multiquadrics-A scattered data approximation scheme with applications to computational fluid-dynamics-I surface approximations and partial derivative estimates. *Comput. Math. Appl.* **1990**, *19*,127–145.
16. Kansa E J. Multiquadrics-A scattered data approximation scheme with applications to computational fluid-dynamics-II solutions to parabolic, hyperbolic and elliptic partial differential equations. *Comput. Math. Appl.* **1990**, *19*,147–161.
17. Kolmogorov A. *É*tude de l' *é*quation de la diffusion avec croissance de la quantit*é* de mati*è*re et son application *à* un probl*è*me biologigue. *Moscow Univ. Bull. Ser. Internat. Sect. A.* **1937**, *1*,1.
18. Liu S, Du Y, Liu X. Numerical studies of a class of reaction-diffusion equations with Stefan conditions. *Int. J.Comput. Math.* **2020**, *97*,9597–979.
19. Liu S, Liu X. Exponential Time Differencing Method for a Reaction-Diffusion System with Free Boundary. *Com. Appl. Math. Comput .* **2023**,1–18.
20. Liu S, Liu X. Numerical methods for a two-species competition-diffusion model with free boundaries. *Math.* **2018**, *6*,72.
21. Liu S. Numerical methods for a class of reaction-diffusion equations with free boundaries. PhD thesis, University of South Carolina, 2019.
22. Liu Y, Qiao Y, Feng X. A stable radial basis function partition of unity method for solving convection-diffusion equations on surfaces. *Eng. Anal. Bound. Elem.* **2023**, *155*, 148–159.
23. Osher S, Fedkiw R P. Level set methods: an overview and some recent results. *J. Comput. Phys.* **2001**, *169*, 463–502.
24. Osher S, Sethian J A. Fronts propagating with curvature-dependent speed: Algorithms based on Hamilton-Jacobi formulations. *J. Comput. Phys.* **1988**, *79*, 12–49.
25. Peng Z, Appelö D, Liu S. Universal AMG accelerated embedded boundary method without small cell stiffness. *J. Sci. Comput.* **2023**, *97*, 1–29.
26. Piqueras M A, Company R, Jódar L. A front-fixing numerical method for a free boundary nonlinear diffusion logistic population model. *J. Comput. Appl. Math.* **2017**, *309*, 473–481.
27. Shaw S B. Radial basis function finite difference approximations of the Laplace-Beltrami operator. **2019**.
28. Tayler A B. Free and moving boundary problems, By J. CRANK. Clarendon, Oxford, 1984. 425 pp.45.00. *J. Fluid. Mech.* **1985**, *158*, 532–533.